Supplementary Information for Atomistic insights into the chemical stability and ionic transport at Li-metal/Li-Argyrodite interfaces

Chantal M. I. Baer*[1,2], Roman Shantsila[2], Łukasz Figiel[1], and Bora Karasulu*[2,3]

[1] *International Institute for Nanocomposite Manufacturing, WMG, University of Warwick, Coventry, CV4 7A*
[2] *Department of Chemistry, University of Warwick, Coventry, CV4 7AL.*
[3] *Energy Innovation Centre, WMG, University of Warwick, Coventry, CV4 7A.*

1 MACE training

The Root Mean Squared errors (RMSEs) on the energies and forces using model 1 of the 3 committee models was obtained by evaluating a dataset of 500 structures taken equidistant from AIMD trajectories at 400 K and 1000 K after each iteration. Iteration 0 represents the initial MD run.

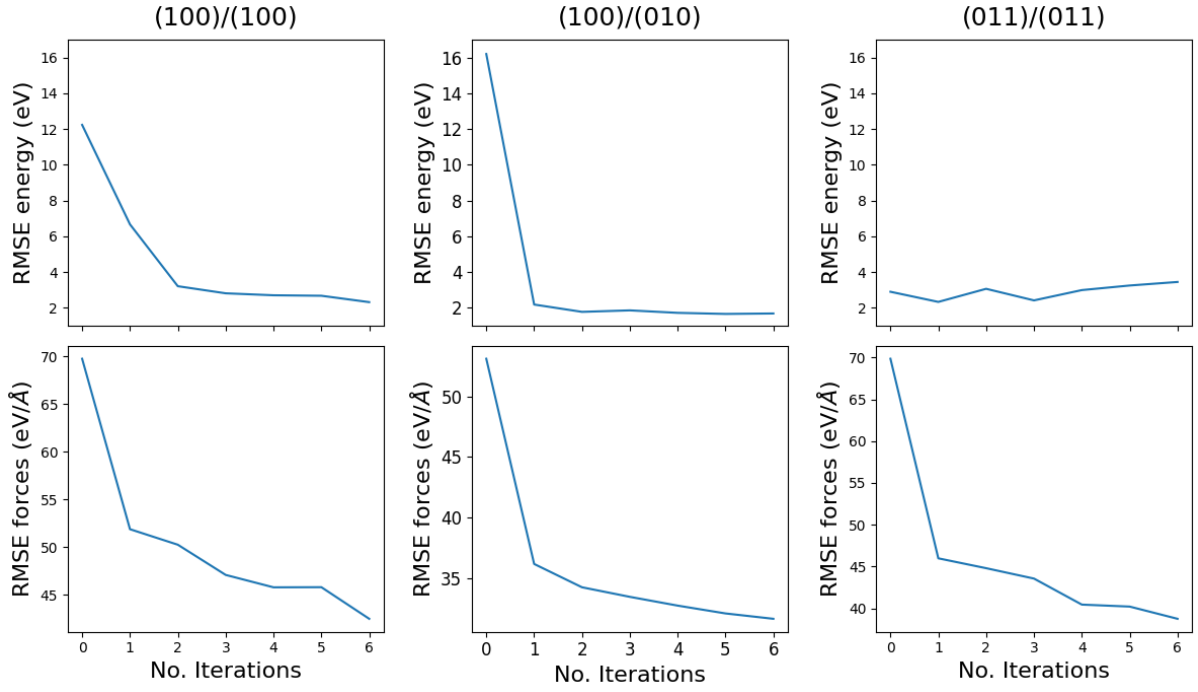

Figure S1: Convergence of the RMSEs of the energies and forces of the MACE models of the (100)/(100), (100)/(010), and (011)/(011) interfaces.

The same test dataset was used to evaluate the final models after the dataset resulting from the active learning process was extended by 100 structures from AIMD runs of the three decomposition products, Li_3P, Li_2S and LiCl, each and trained using the multi-head fine-tuning protocol.

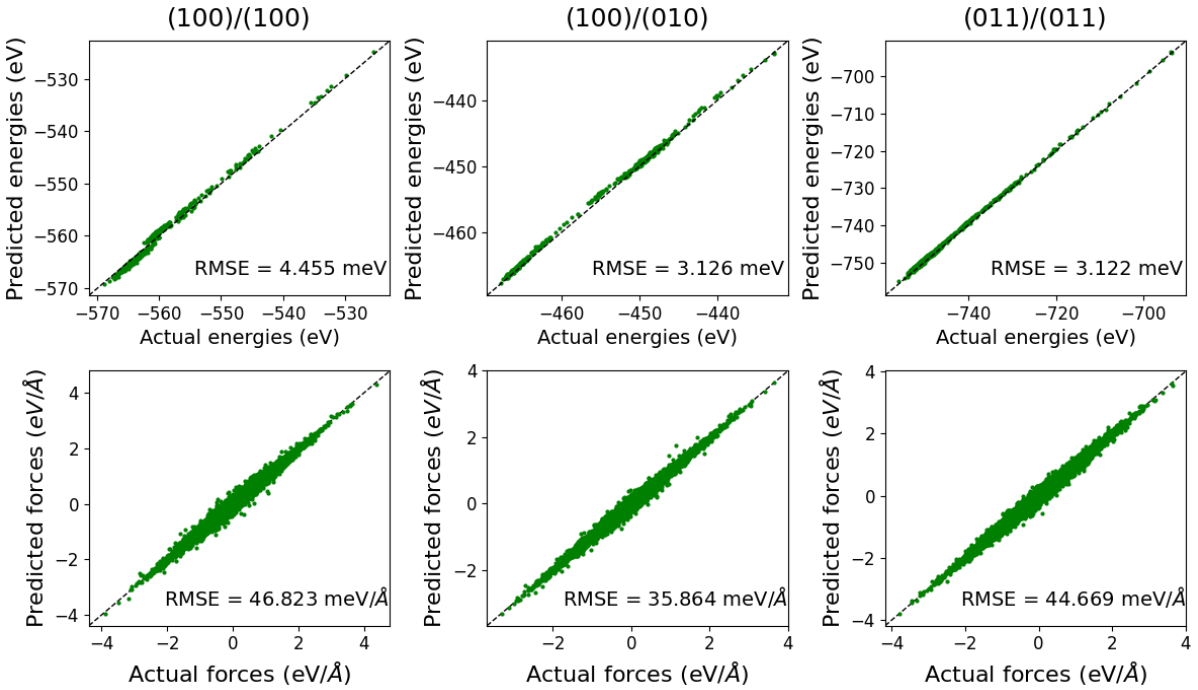

Figure S2: RMSEs of the energies and forces of the three MACE models trained on bulk Li-metal and Li-Argyrodite bulk structures each, and the respective structures of the (100)/(100), (100)/(010), and (011)/(011) interfaces.

The average radial distribution function (RDF) was used to validate that the models correctly capture the chemistry happening at the interfaces, as shown in Figure S3. It was found that the discrepancy between the RDFs is mainly due to a poor description of the S-P bond behaviour, so the S-P RDF was also compared (see Figure S4).

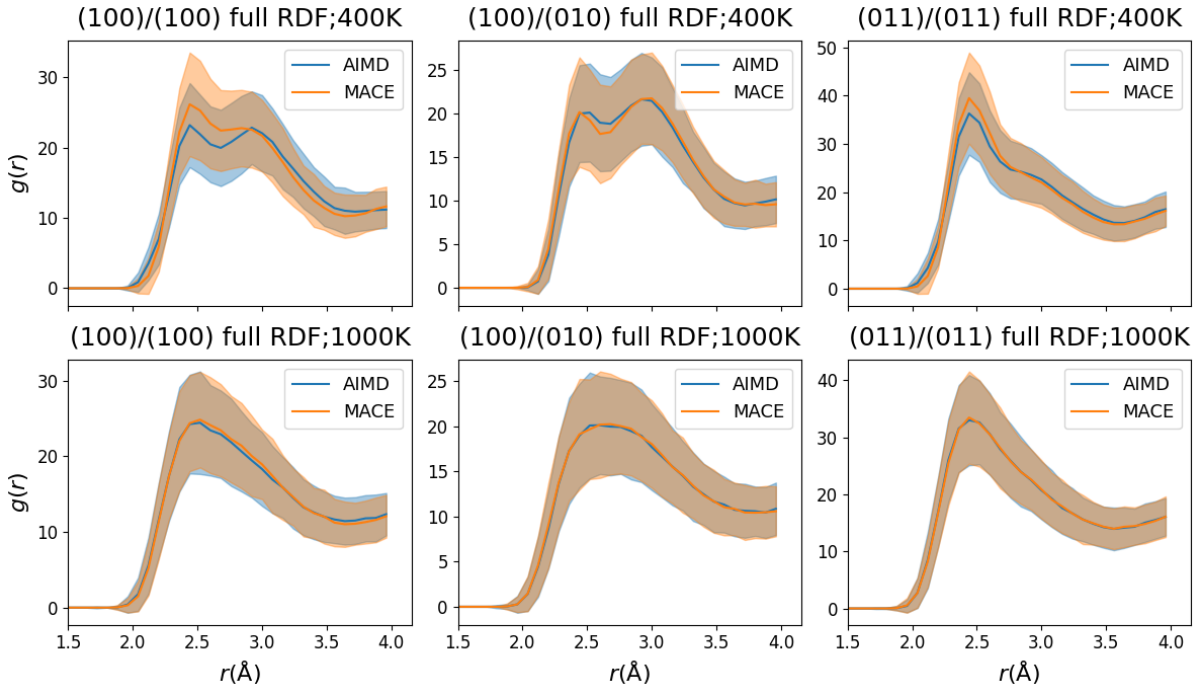

Figure S3: Full RDF of the (100)/(100), (100)/(010), and (011)/(011) interfaces run with AIMD (blue) and MLMD (orange) at 400 K and 1000 K for 20 ps. The 95% confidence interval is highlighted for both cases to compare the accuracy of the ML model to DFT.

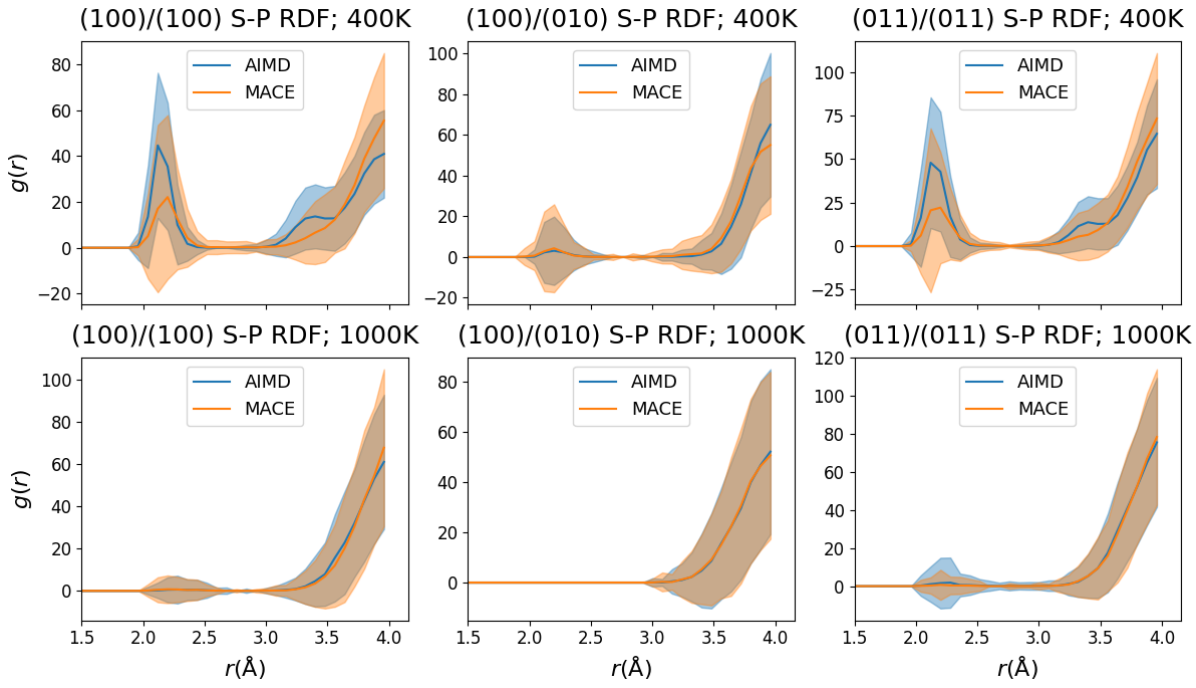

Figure S4: Partial RDF for the S-P pair of the (100)/(100), (100)/(010), and (011)/(011) interfaces run with AIMD (blue) and MLMD (orange) at 400 K and 1000 K for 20 ps. The 95% confidence interval is highlighted for both cases to compare the accuracy of the ML model to DFT.

To evaluate the bulk behaviour of the three MACE models, each model was evaluated on a dataset of 400 structures of bulk Li-Argyrodite, with 100 structures taken equidistant from 400 K, 600 K, 800 K, and 1000 K AIMD simulations.

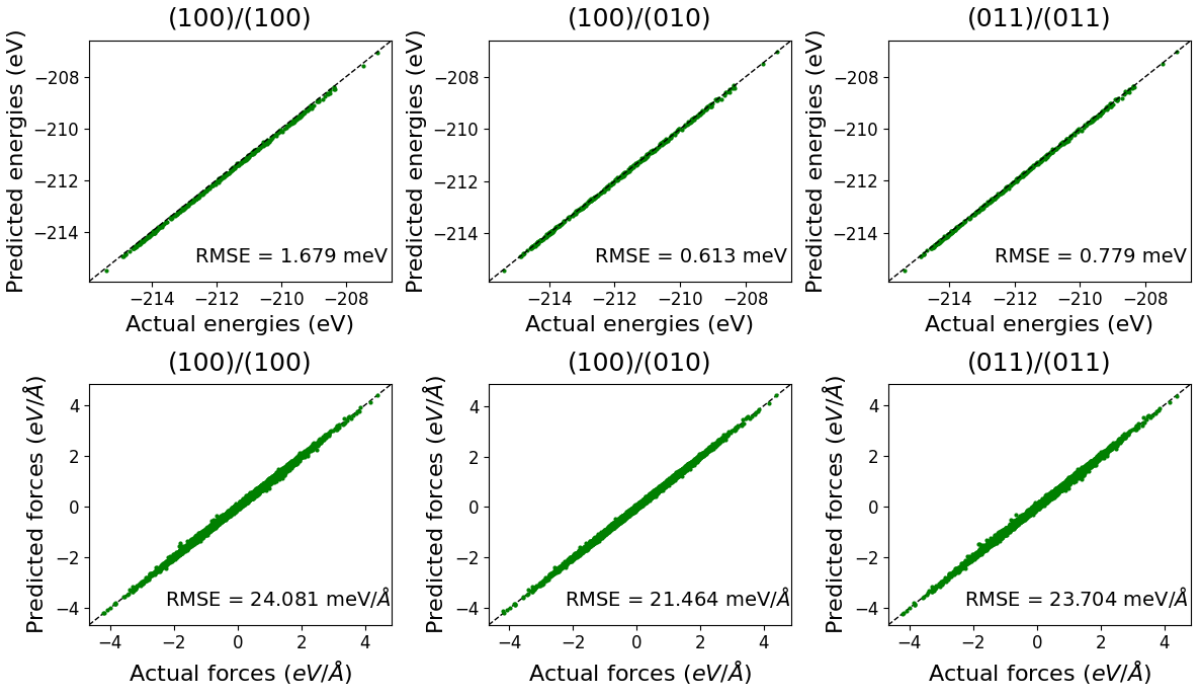

Figure S5: RMSEs of the energies and forces for the three MACE models used on a test set of 400 bulk Li-Argyrodite structures, to evaluate how well they reproduce the bulk properties.

2 Bulk Li-Argyrodite

The *Kinisi* code was used to obtain the diffusion coefficient at 400 K, 600 K, 800 K, and 1000 K by fitting a linear model to the mean squared displacement (MSD) data from the MACE MD simulations. The start of the diffusive regime was set as 5 ps for all four temperatures.

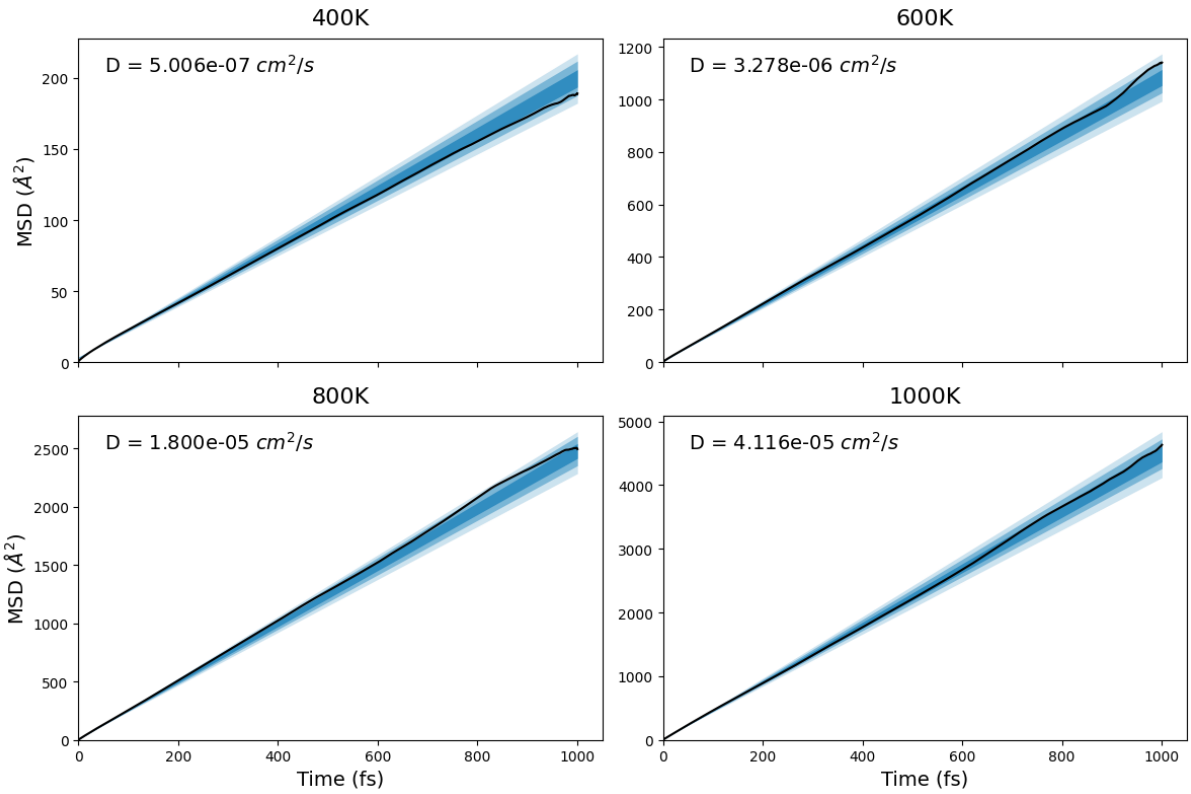

Figure S6: MSD vs time plot for bulk Li-Argyrodite at 400 K, 600 K, 800 K, and 1000 K from MACE MD trajectories, with respective 95% uncertainty interval calculated using *kinisi*.

When calculating the mean-squared total displacement (MSTD) of the centre of mass, there is only one single 'system particle' observed, which results in poor statistics compared to the calculation of the MSD with the number of 'system particles' being the number of diffusing atoms. To improve the statistics, 20 simulations with different random seeds were run using MACE at each temperature, 400 K, 600 K, 800 K, and 1000 K, and passed to *kinisi* with the keyword 'dtype = identical". Furthermore, we increased the number of system particles to 40 by setting "system_particles = 40", knowing that there are at least 20 uncorrelated Li-ions in the system.

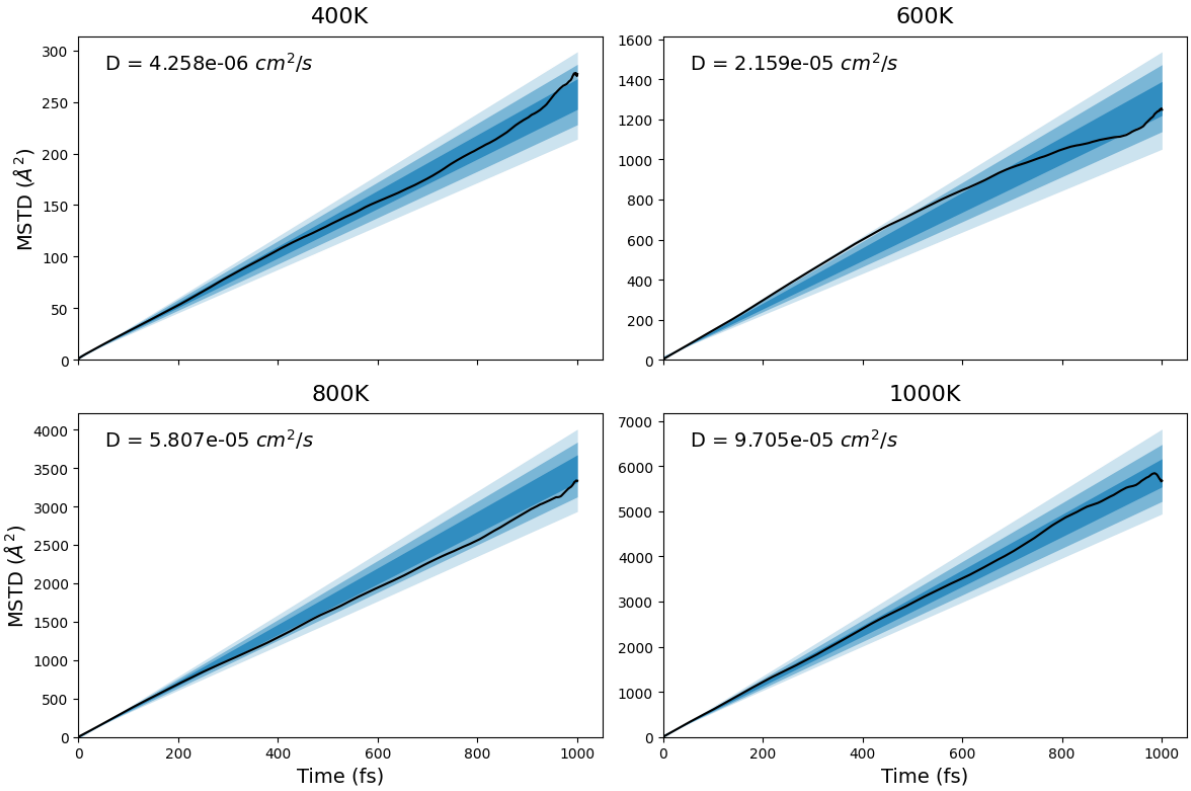

Figure S7: MSTD vs time plot, i.e. centre-of-mass diffusion, for bulk Li-Argyrodite at 400 K, 600 K, 800 K, and 1000 K from MACE MD trajectories with respective 95% uncertainty interval, obtained from 20 replicas at different seeds and using 40'system_particles' in *kinisi*.

3 Surfaces

Points to consider when creating surface models: 1. Different surfaces are created depending on the Miller plane along which the surfaces are cut. 2. There are different surface terminations for each Miller index. Furthermore, the surface slabs must be symmetrised to calculate a reliable surface formation energy (γ_{surf}) and not the average of two different surfaces. γ_{surf} is calculated according to equation 4 in the main text.

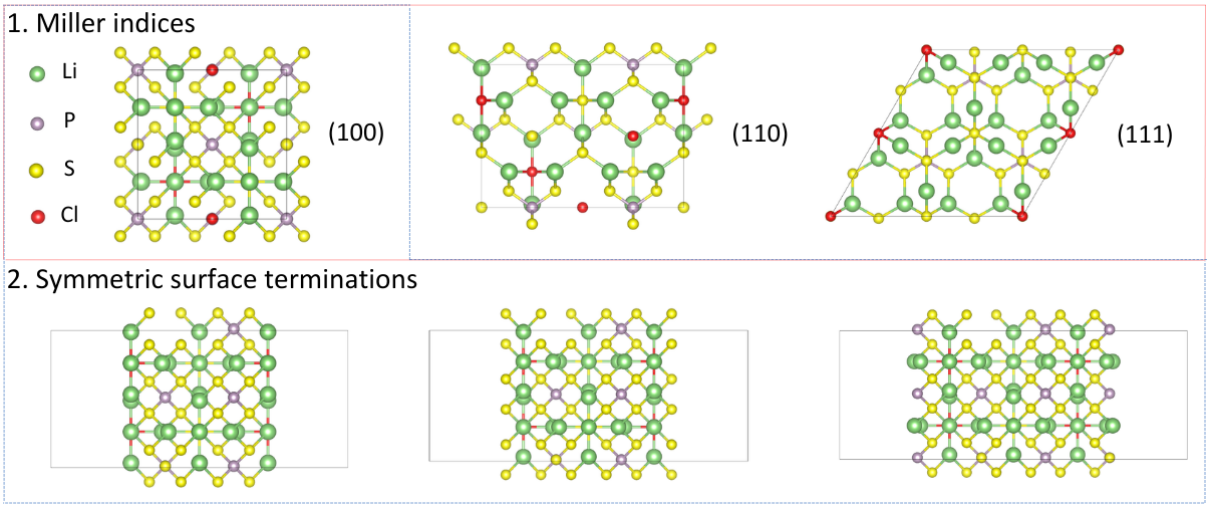

Figure S8: Examples of different surfaces created by cutting Li-Argyrodite along 1. different Miller Planes of (100), (010), and (111) and 2. three different surface terminations of the (100) Miller plane.

Here we created all possible symmetric surface terminations for the Miller indices (100), (010), (001), (110), (101), (011), (111) using *Pymatgen's* 'SlabGenerator' to cut a slab along the desired Miller plane and using the 'nonstoichiometric_symmetrized_slab' function to find the symmetric terminations. A total of 28 surface models were created and relaxed with DFT. The surface formation energies of all resulting surfaces are compared in Figures S9 and S10.

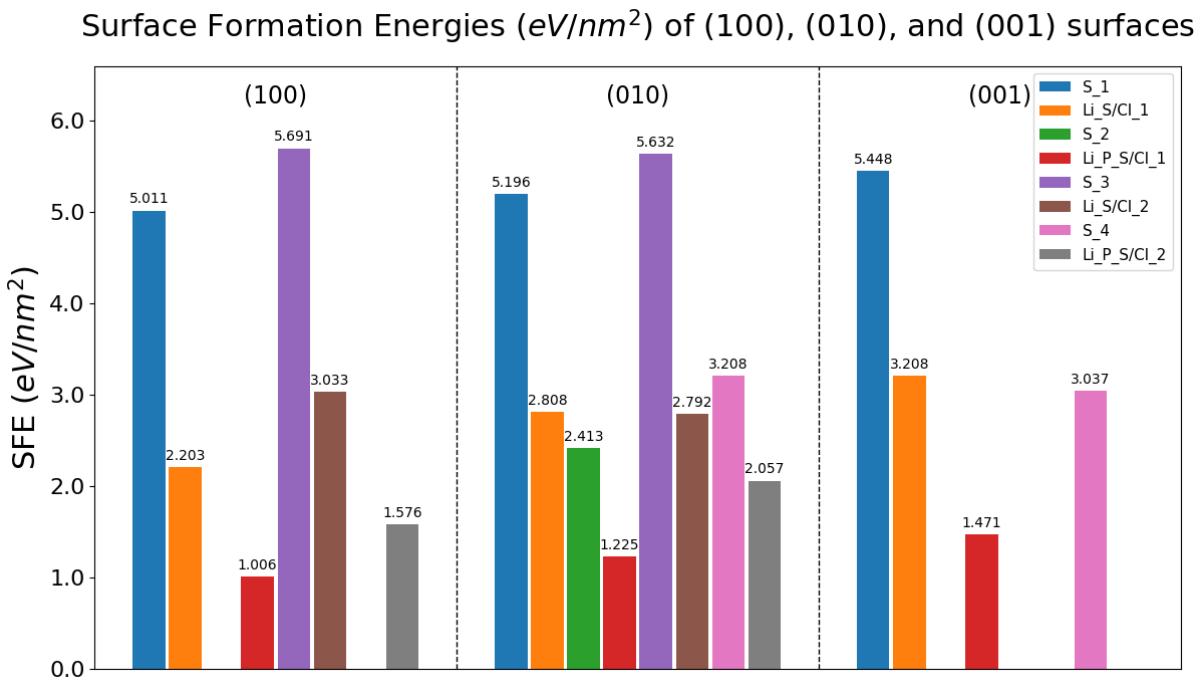

Figure S9: The resulting γ_{surf} for the Miller indices (100), (010), and (001). Each bar represents a unique surface slab and the colour indicates the atoms on the outer layer. The height of the bars gives the γ_{surf} in eV/nm^2.

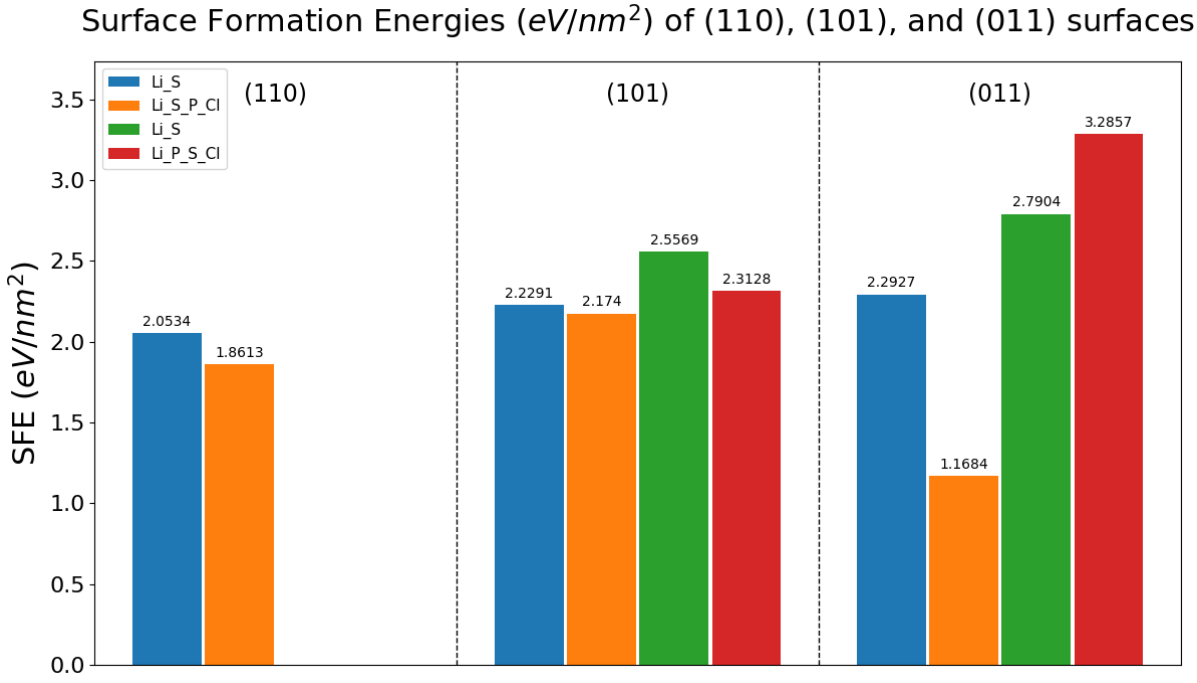

Figure S10: The resulting γ_{surf} for the Miller indices (110), (101), and (011). Each bar represents a unique surface slab and the colour indicates the atoms on the outer layer, i.e. the surface termination. The height of the bars gives the γ_{surf} in eV/nm^2.

4 Interface Creation

For charge-balancing, the types of atoms to be deleted were considered first to ensure that the least possible number of atoms are removed. The charge is determined from the exact composition, taking into account the oxidation state of each species in the system, i.e. Li: +1, P:+5, S:-2, and Cl:-1. For the (100) surface, the composition is $Li_{40}P_8S_{32}Cl_6$, leading to a charge of +10. The minimum number of atoms to be deleted is thus two P atoms. To determine which specific P-atoms to delete, a configuration enumeration was run, replacing P-atoms on the outer layers with a vacancy and obtaining the single point energies of all possible combinations of 2 vacancies to determine the most energetically favourable removal of P-atoms.

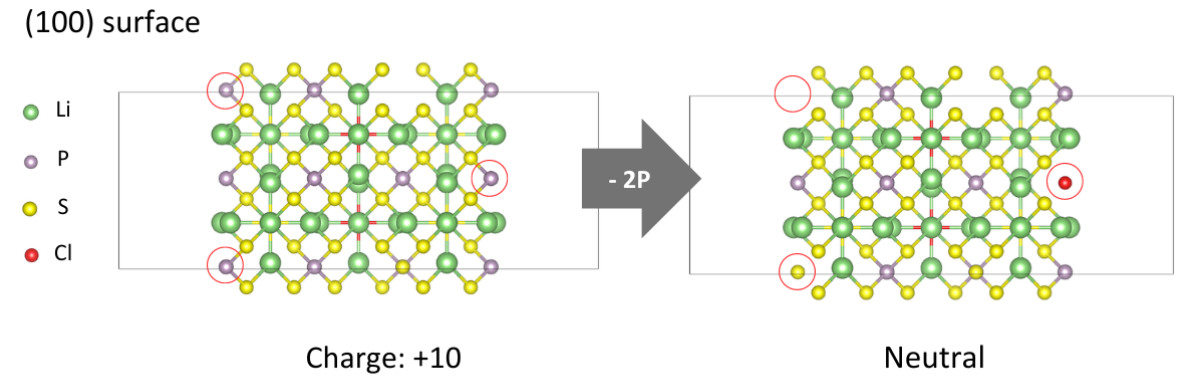

Figure S11: Charge-balancing the symmetric and non-stoichiometric Li-Argyrodite (100) Surface with a charge of +10 by deleting the 2 energetically most favourable P atoms from the surface layers.

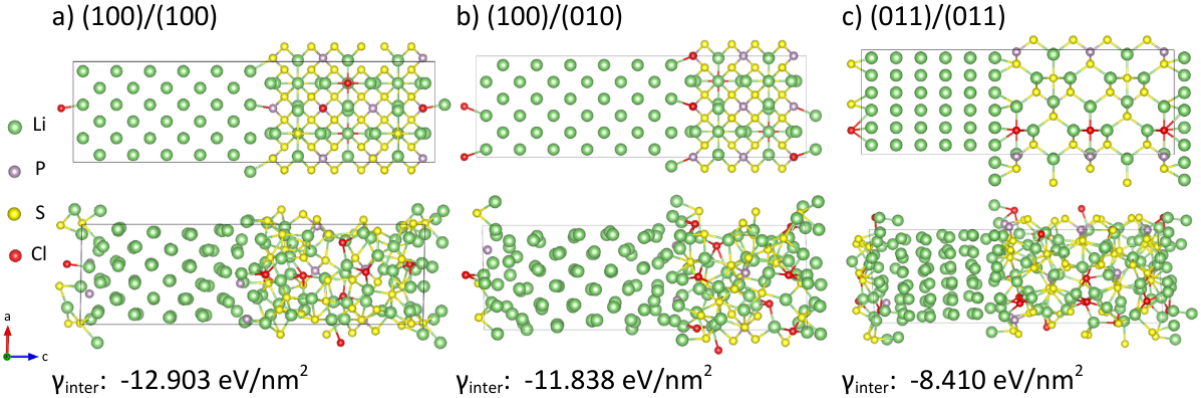

Figure S12: Li-metal/Li-Argyrodite (100)/(100), (100)/(010), and (011)/(011) interfaces before (top) and after (bottom) geometry optimisation with DFT before charge-balancing. The miller plane for Li-metal was chosen so that the interface would have minimal lattice mismatch, reducing the strain in the model, which is introduced when fitting two surfaces with different lattice parameters into one supercell. The interface formation energy (γ_{inter}), calculated using equation 9 in the main text, is given for each structure in eV/nm^2.

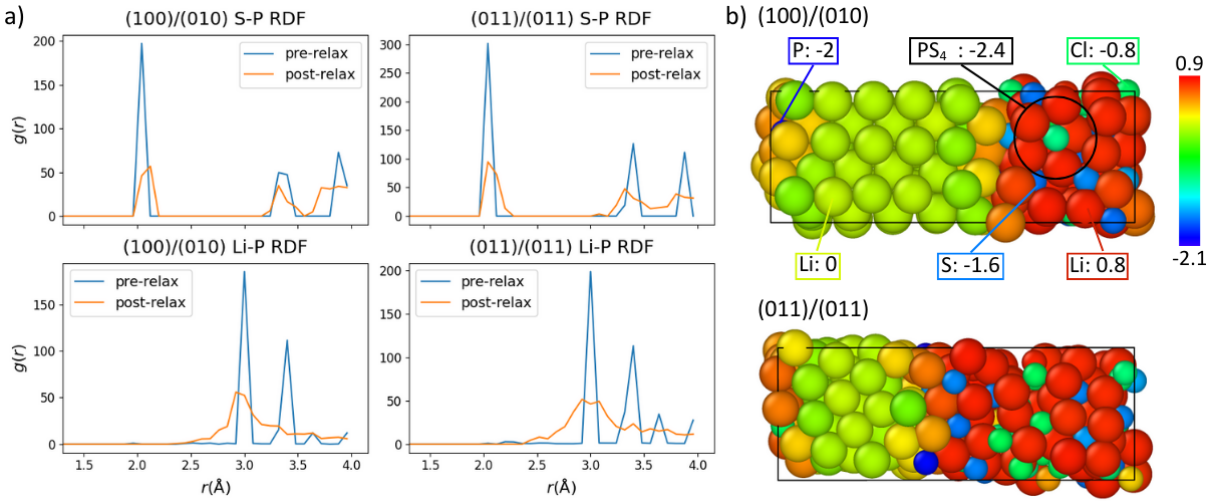

Figure S13: a) Partial RDFs of the P-S (top) and P-Li (bottom) bond lengths of the (100)/(010) and (011)/(011) interfaces before and after the geometry optimisation. b) DDEC6 charge partitioning of the optimised (100)/(010) and (011)/(011) interface.

5 MLMD results

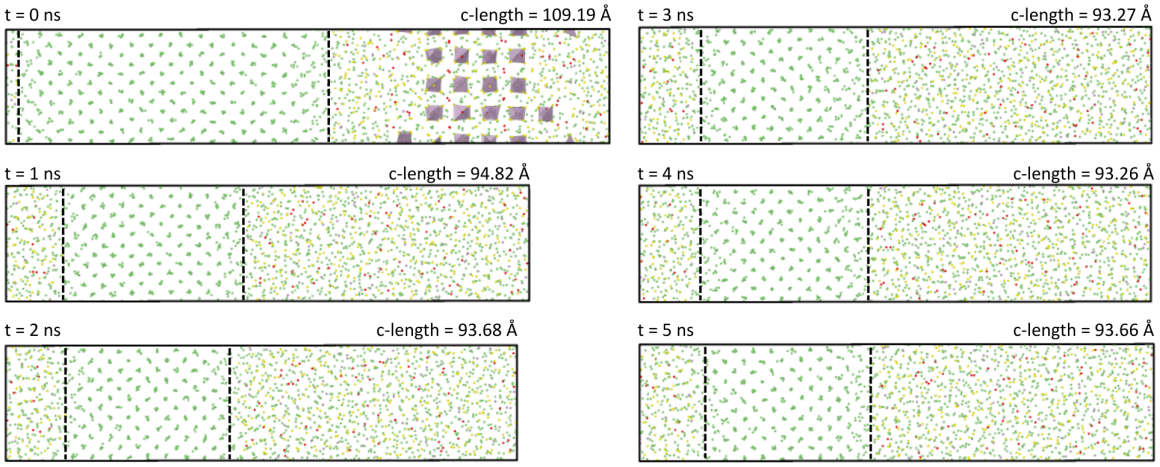

Figure S14: Snapshots of the 5 ns MD trajectory of the (100)/(100) interface at 300 K, taken every ns. The vertical thick lines indicate the position of the interface, determined by the non-Li atom that diffused furthest into the Li-metal. The thin lines show the crystalline regime which grows throughout the simulation.

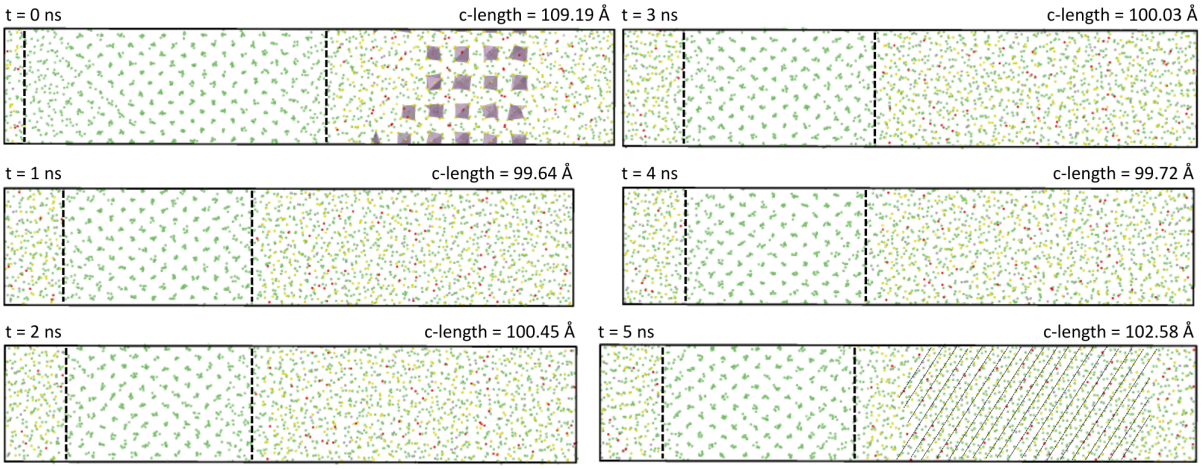

Figure S15: Snapshots of the 5 ns MD trajectory of the (100)/(100) symmetric interface at 400 K, taken every ns. The vertical thick lines indicate the position of the interface, determined by the non-Li atom that diffused furthest into the Li-metal. The thin lines show the crystalline regime which grows throughout the simulation.

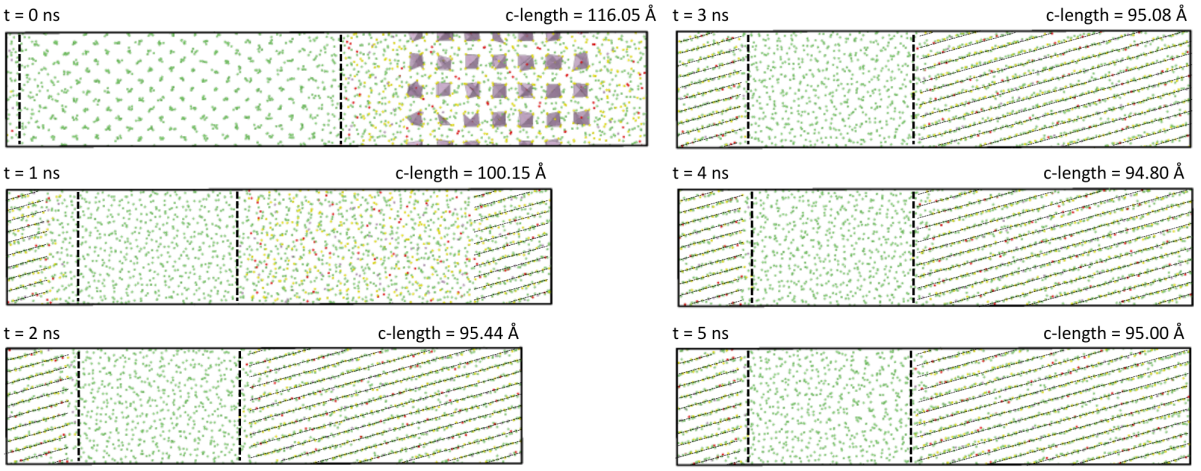

Figure S16: Snapshots of the 5 ns MD trajectory of the (100)/(010) interface at 400 K, taken every ns. The vertical thick lines indicate the position of the interface, determined by the non-Li atom that diffused furthest into the Li-metal. The thin lines show the crystalline regime which grows throughout the simulation.

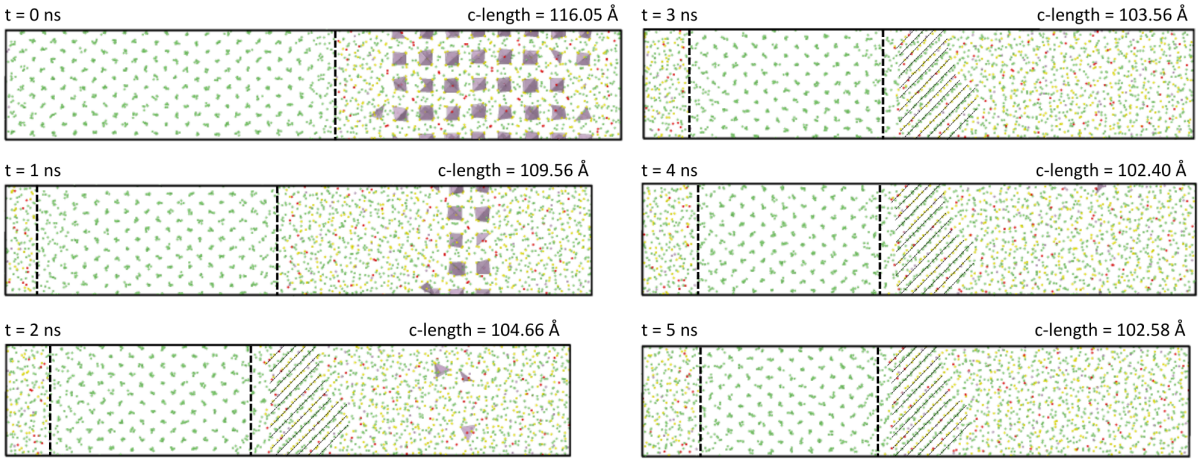

Figure S17: Snapshots of the 5 ns MD trajectory of the (100)/(010) interface at 300 K, taken every ns. The vertical thick lines indicate the position of the interface, determined by the non-Li atom that diffused furthest into the Li-metal. The thin lines show the crystalline regime which grows throughout the simulation.

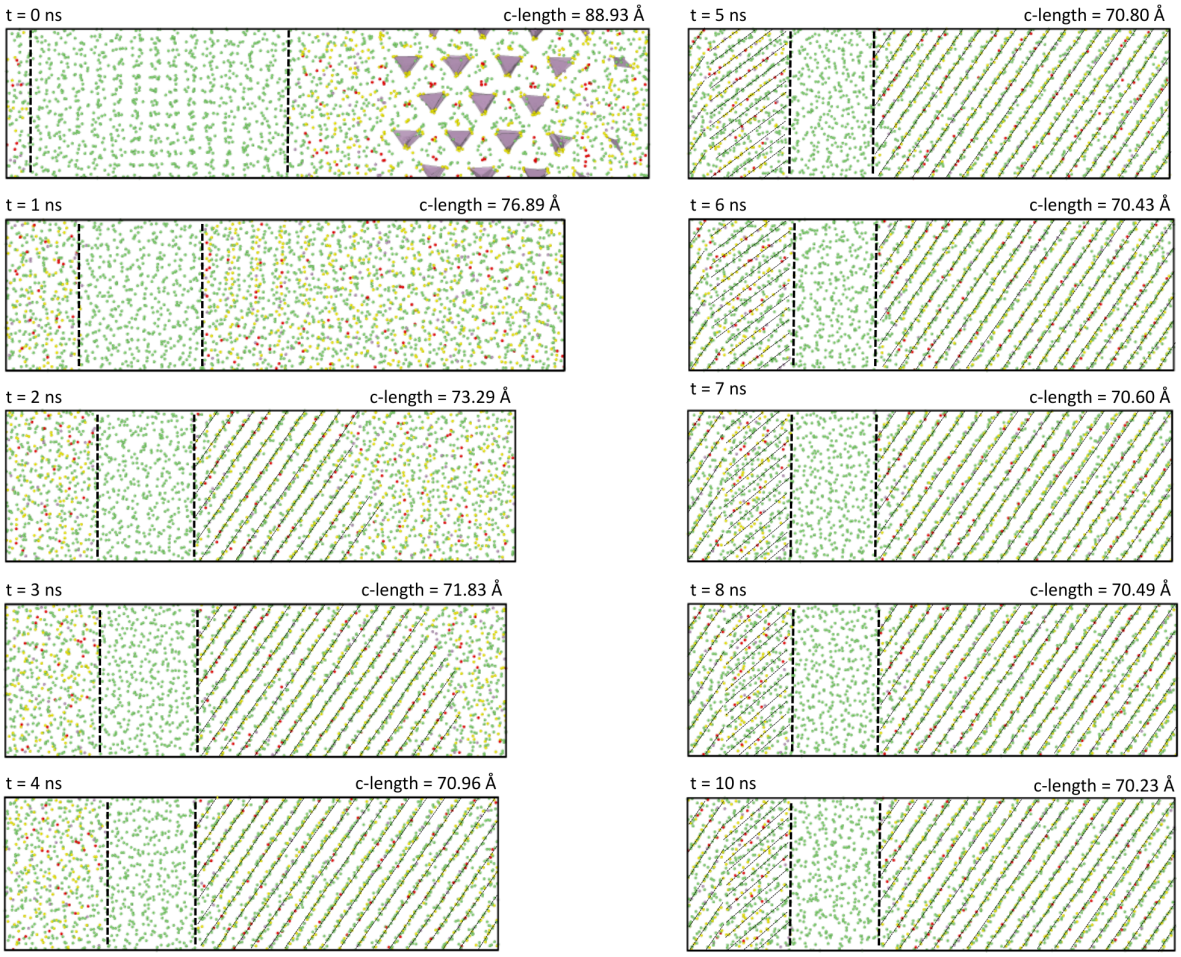

Figure S18: Snapshots of the 10 ns MD trajectory of the (011)/(011) interface at 400 K, taken every ns (excluding 9 ns). The vertical thick lines indicate the position of the interface, determined by the non-Li atom that diffused furthest into the Li-metal. The thin lines show the crystalline regime which grows throughout the simulation.

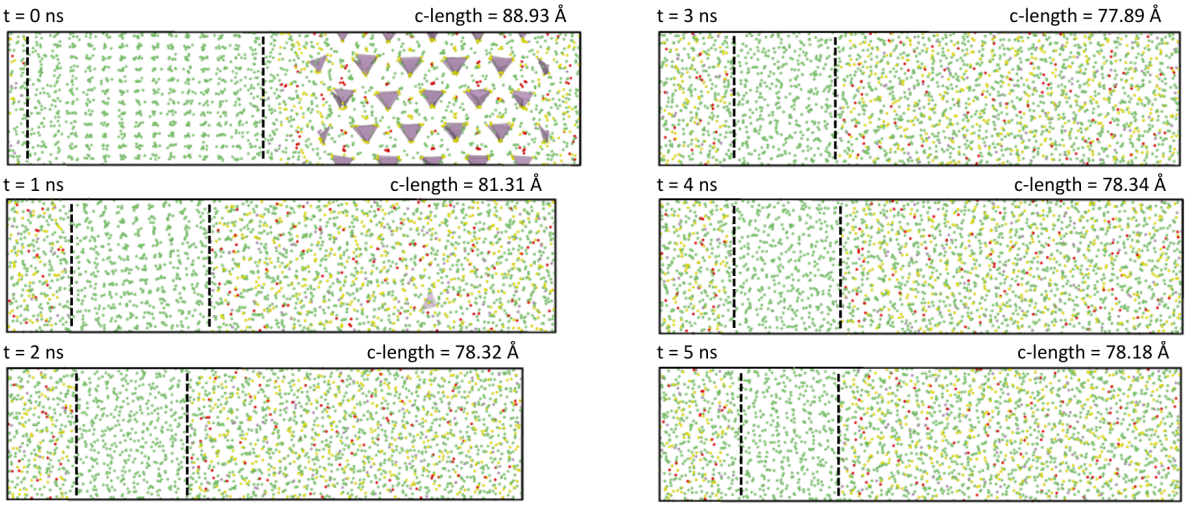

Figure S19: Snapshots of the 5 ns MD trajectory of the (011)/(011) interface at 300 K, taken every ns. The vertical thick lines indicate the position of the interface, determined by the non-Li atom that diffused furthest into the Li-metal. The thin lines show the crystalline regime which grows throughout the simulation.

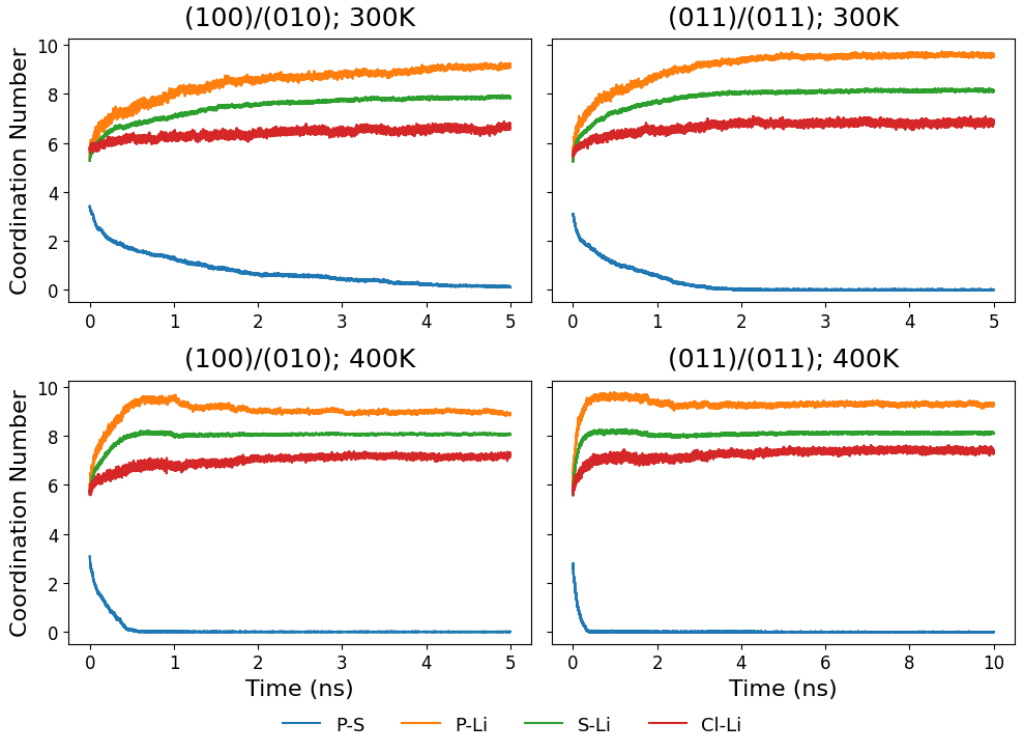

Figure S20: Evolution of the coordination numbers of the S-P, P-Li, S-Li, and Cl-Li bonds of the (100)/(010) and (011)/(011) interfaces at 300 K and 400 K.

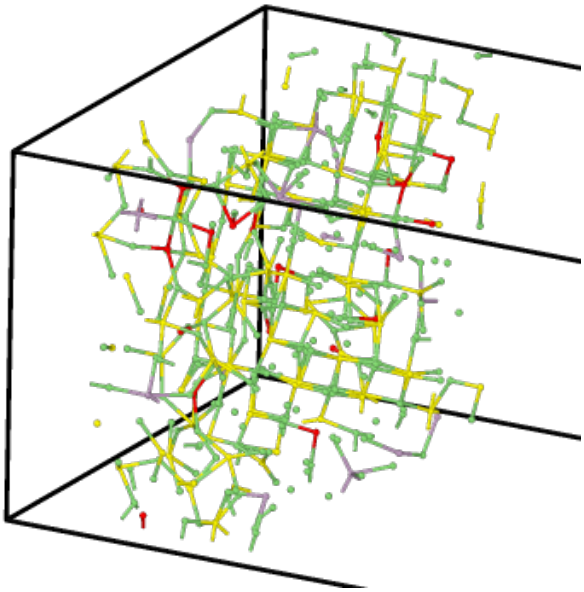

Figure S21: Antifluorite crystal structure of the crystalline phase of different orientation of the (011)/(011) interface at 10 ns.

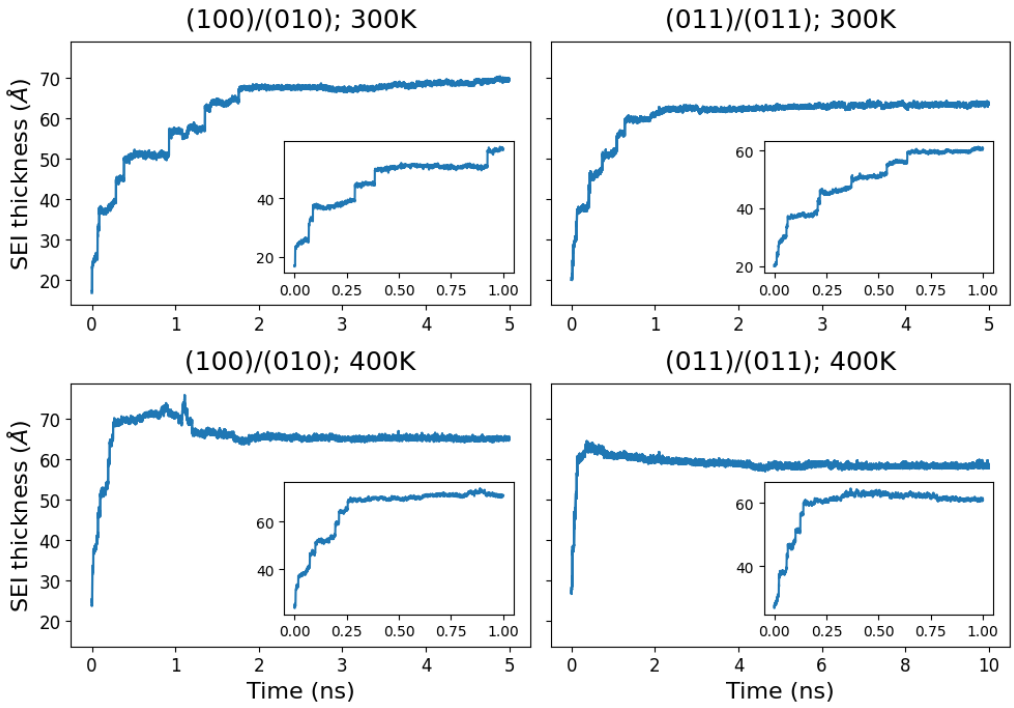

Figure S22: Solid electrolyte interface (SEI) thickness of the (100)/(010), and (011)/(011) interfaces at 300 K and 400 K, each. The thickness was calculated by obtaining the distance between the edges of the intact Li-Argyrodite, determined by the position of the most outer, intact PS_4 polyhedra, and the edge interface with Li-metal, determined by the position of the most outer non-Li atom.

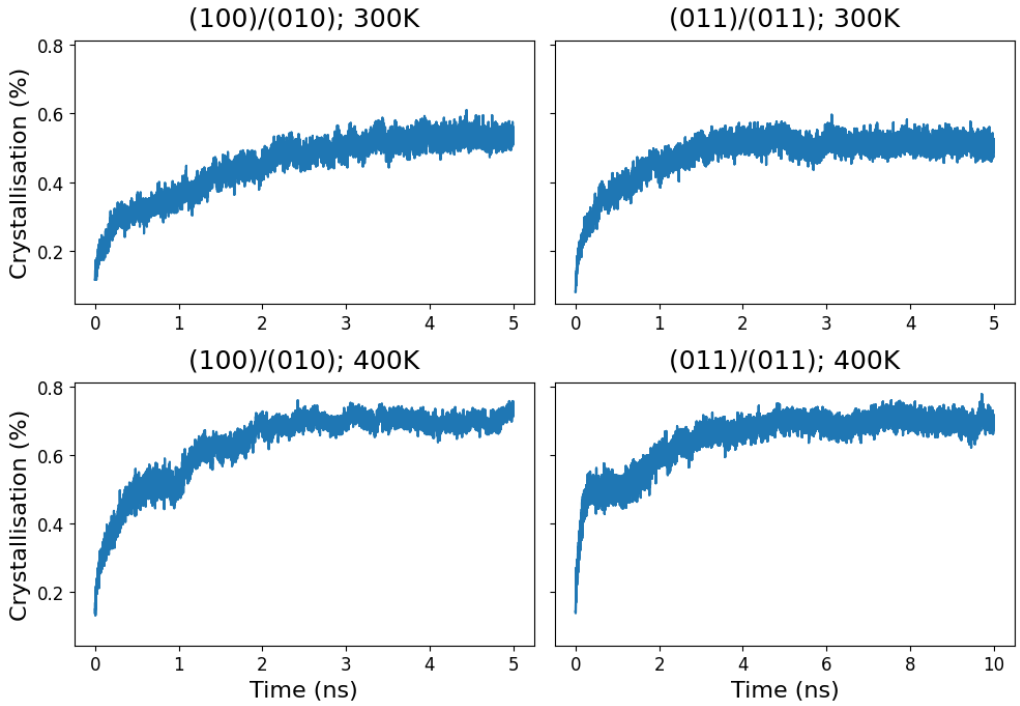

Figure S23: Crystallisation ratio (in %) of the SEI of the (100)/(010) and (011)/(011) interfaces at 300 K and 400 K. Calculated by determining the number of S atoms with a coordination number of 8 (as in the antifluorite structure) and dividing by the total number of S atoms.

Table S1: End time of the decomposition (D) and start and end time of crystallisation (C) for the (100)/(100) interfaces with different P removed for charge-balancing at 400 K.

System	End D (ns)	Start C (ns)
Original	0.39	0.24
Charge balancing 1	0.39	0.23
Charge balancing 2	0.47	0.41

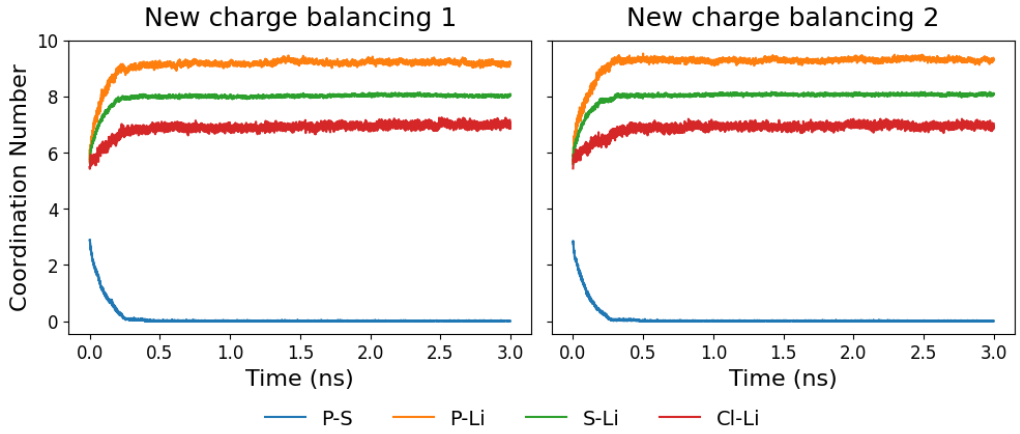

Figure S24: Evolution of the coordination numbers of the S-P, P-Li, S-Li, and Cl-Li bonds of two (100)/(100) interface models with different P removed for charge-balancing at 400 K.

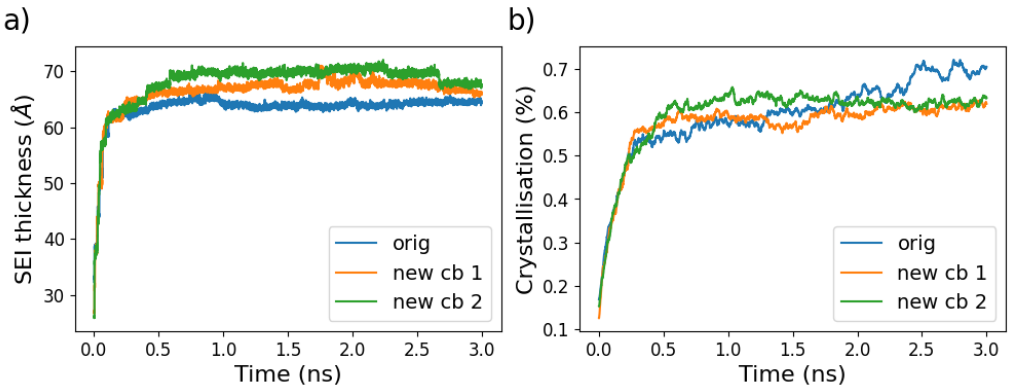

Figure S25: a) Solid electrolyte interface (SEI) thickness and b) Crystallisation (in %) of the SEI of the two (100)/(010) interface models with different P removed for charge-balancing at 400 K. An exponential moving average was used for the crystallisation fraction.

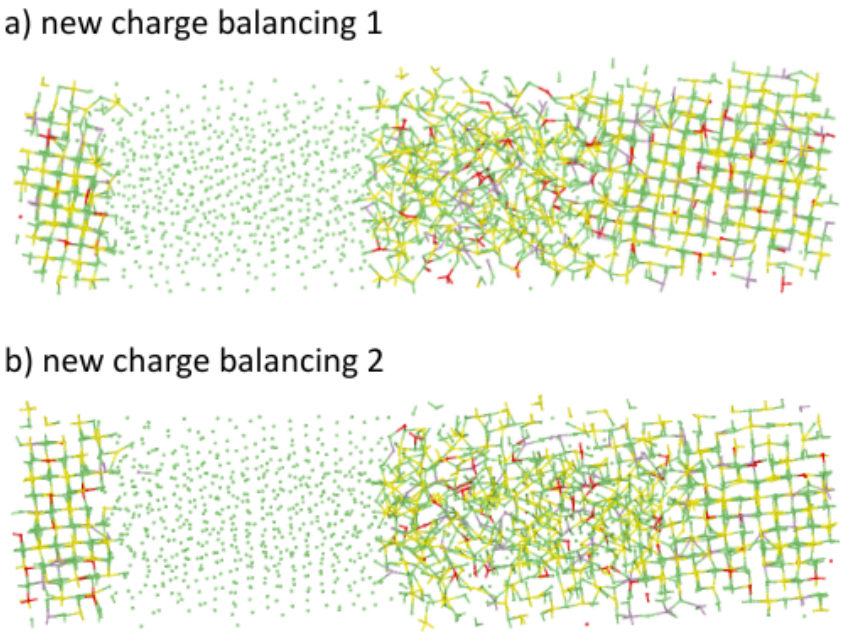

Figure S26: Antifluorite crystal structure of the two (100)/(100) interface models with different P removed for charge-balancing after 3 ns simulation at 400 K.

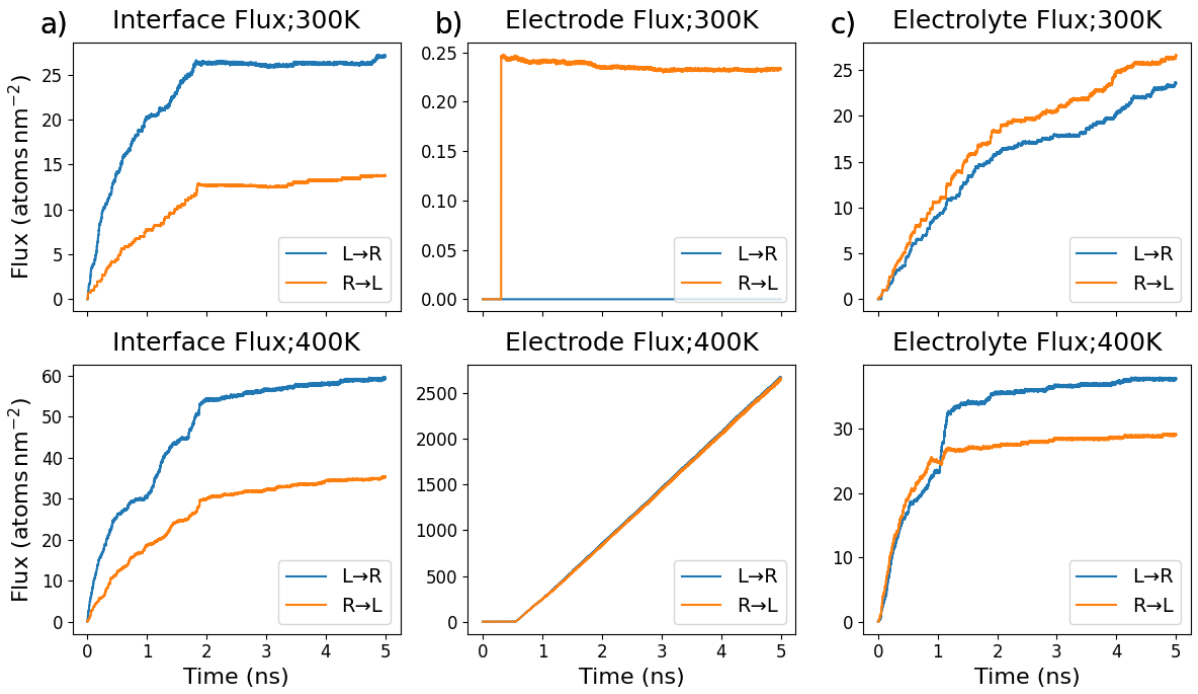

Figure S27: Interface, electrode, and electrolyte flux of Li-ions over the 5 ns trajectory of the (100)/(010) interface at 300 K and 400 K.

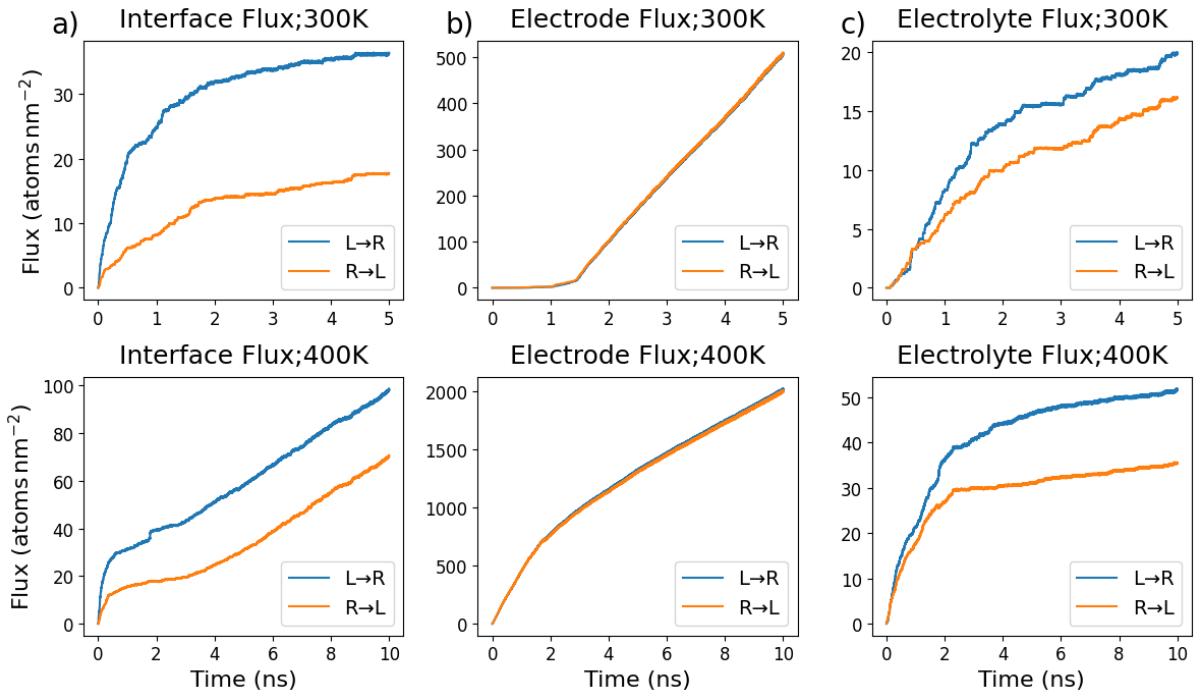

Figure S28: Interface, electrode, and electrolyte flux of Li-ions of the (011)/(011) interface over the 5 ns at 300 K and 10 ns at 400 K.

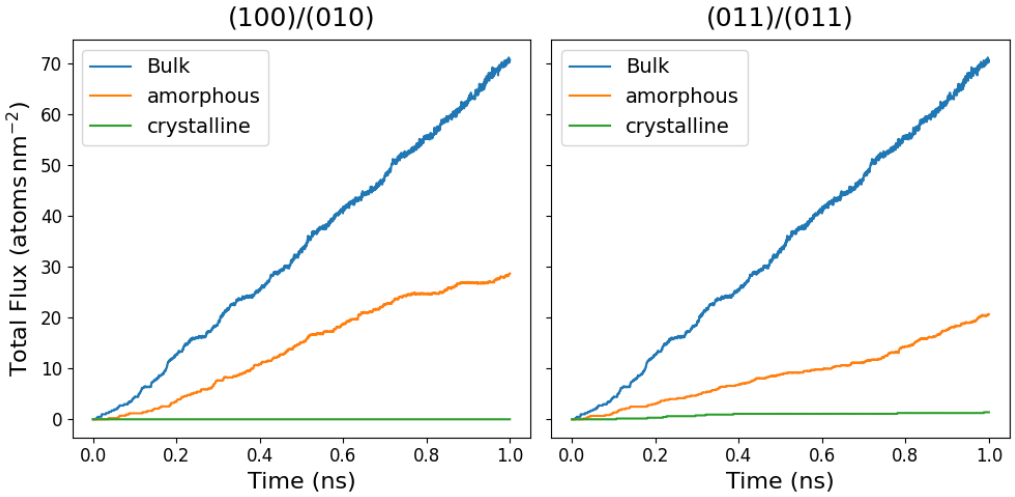

Figure S29: Total flux in atoms/nm^{2}ns of Li-Argyrodite bulk along with the amorphous and crystalline SEI for the (100)/(010) and (011)/(011) interfaces, tracked for 1 ns.

Table S2: Average flux from left to right (L→R) and right to left (R→L) of the (100)/(100), (100)/(010), and (011)/(011) interfaces calculated at the interface, the centre of the electrode, and the centre of the electrolyte.

Interface	Temp (K)	Position	Flux L→R ($atoms/(nm^2ns)$)	Flux R→L ($atoms/(nm^2ns)$)
(100)/(100)	300	Interface	5.834	2.572
		Electrode	0.0	0.0
		Electrolyte	3.170	3.261
	400	Interface	13.010	9.021
		Electrode	1.088	0.544
		Electrolyte	7.435	6.301
(100)/(010)	300	Interface	5.408	2.751
		Electrode	0.0	0.0
		Electrolyte	4.709	5.315
	400	Interface	11.919	7.090
		Electrode	53.439	53.191
		Electrolyte	7.569	5.829
(011)/(011)	300	Interface	7.269	3.548
		Electrode	101.694	102.039
		Electrolyte	3.996	3.238
	400	Interface	9.801	7.027
		Electrode	201.159	199.618
		Electrolyte	3.529	5.147